Published in final edited form as:
Anal Chem. 2011 June 1; 83(11): 4137–4146. doi:10.1021/ac2001498.

Infrared and Raman Spectroscopic Studies of the Antimicrobial Effects of Garlic Concentrates and Diallyl Constituents on Foodborne Pathogens

Xiaonan Lu[1,3], **Barbara A. Rasco**[1,*], **Dong-Hyun Kang**[1], **Jamie M.F. Jabal**[2], **D. Eric Aston**[2], and **Michael E. Konkel**[3]

[1]School of Food Science, Washington State University, Pullman 99163, USA

[2]Department of Chemical and Materials Engineering, University of Idaho, Moscow 83844, USA

[3]School of Molecular Biosciences, Washington State University, Pullman, WA 99163, USA

Abstract

The antimicrobial effects of garlic (*Allium sativum*) extract (25, 50, 75, 100, and 200 μl/ml) and diallyl sulfide (5, 10 and 20 μM) on *Listeria monocytogenes* and *Escherichia coli* O157:H7 cultivated in tryptic soy broth at 4, 22 and 35°C for up to 7 days were investigated. *L. monocytogenes* was more resistant to garlic extract and diallyl compounds treatment than *E. coli* O157:H7. Fourier transform Infrared (FT-IR) spectroscopy indicated that diallyl constituents contributed more to the antimicrobial effect than phenolic compounds. This effect was verified by Raman spectroscopy and Raman mapping on single bacteria. Scanning electron microscope (SEM) and transmission electron microscope (TEM) showed cell membrane damage consistent with spectroscopic observation. The degree of bacterial cell injury could be quantified using chemometric methods.

Keywords

Raman spectroscopy; infrared spectroscopy; garlic; diallyl sulfides; *Escherichia coli* O157:H7; *Listeria monocytogenes*

Listeria monocytogenes is ubiquitous in the environment and has been found in many species of domestic and wild animals, plants, soil and water sources. It can tolerate temperatures between 3 and 45°C, pH between 5.4 and 9.6, high temperature short time pasteurization processes, and long periods of freezing. Enterohemorrhagic *Escherichia coli* (EHEC) are pathogenic bacteria that cause human illness following direct contact with infected humans or animals, or indirectly after consuming contaminated food or water [1].

Controlling foodborne pathogens is critical and natural plant extracts are potential food preservatives with high consumer acceptability. Polyphenolic compounds that bind to plant sugars as glucosides [2, 3] have antimicrobial activity. Garlic (*Allium sativum*) and onion (*Allium cepa*) also contain organosulfur compounds that possess antibacterial, antioxidant and anti-inflammatory activities [4-7]. Allicin [8, 9], ajoene [10], and diallyl sulfides [5-7] are mainly responsible for the bioactive properties; but phenolic compounds and steroid saponins in *Allium* species may behave synergistically [3, 4].

*Corresponding author. P.O. Box 646376 School of Food Science Washington State University Pullman, WA 99163, USA Tel.: +1-509-335-1858; fax: +1-509-335-4815 rasco@wsu.edu.

SUPPORTING INFORMATION AVAILABLE Additional information as noted in text.

Understanding the mechanism of antimicrobial activity is critical if these compounds are to be promoted as food additives. Most antimicrobial agents alter microbial cell membranes causing leakage or autolysis thus inhibiting growth or causing cell death. Gene activity and protein expression [11] and changes in spectral features [12] are common methods for study. Vibrational spectroscopy provides a rapid and noninvasive alternative to studying injury and changes in bacterial cell membranes [13-17]. Infrared and Raman spectroscopies could provide complementary spectral features of bacteria [18]. Mid-infrared and Raman spectroscopy can identify and differentiate bacteria [14, 19, 20], and detect bacterial injury from: thermal and cold treatment [12], bacteriocin [21], chemical and antibiotic treatment [22-24], acid and alkaline treatment [12], and an exposure to silver nanoparticles [25].

Spectral interference from food matrices pose a problem and techniques to overcome this include capture with immunomagnetic beads [26] and filtration [27] often coupled with spectroscopic analysis. Raman spectroscopy can target single bacterial cells using confocal microscopy and mapping techniques [16]. New techniques to improve Raman sensitivity such as a shell-isolated substrate designed for surface enhancement of Raman signals for bioanalytes can overcome poor reproducibility of surface enhanced Raman scattering (SERS) substrates [28]. In current study, cell injury caused by garlic and its diallyl constituents on Gram positive *Listeria monocytogenes* and Gram negative *Escherichia coli* O157:H7 were studied. SEM and TEM were used to verify structural cell injury.

EXPERIMENTAL SECTION

Chemicals and reagents

Folin-Ciocalteu reagent, gallic acid, methanol, 2,2 diphyenyl-1-picrylhydrazyl (DPPH), 6-hydroxy-2,5,7,8-tetramethyl-2-carboxylic acid (Trolox), acetonitrile, and tetrahydrofuran were obtained from Sigma-Aldrich (HPLC grade, St. Louis, MO, USA). Sodium carbonate was purchased from J.T. Baker Inc. (Phillipsburg, NJ, USA). Diallyl sulfide (purity 98%) was purchased from Sigma.

Reverse-phase HPLC (Agilent 1100 HPLC system) with a diode-array detector (240 nm) (Palo Alto, CA, USA) was used to check purity and stability of diallyl sulfide (10 μl injection volume) by separation on a Nova-Pak C_{18} column (4 μm, 4.6 ×150 mm, Waters Corporation, Milford, MA, USA) with a symmetry C_{18} guard column (5 μm, 3.9 × 20 mm, Waters) and 70:27:3 (v/v: acetonitrile to water to tetrahydrofuran) mobile phase at a 1 ml/min.

Culture preparation

Bacterial strains were obtained from the School of Food Science culture collection Washington State University (Pullman, WA, USA): *E. coli* O157:H7 (ATCC 35150, ATCC 43889 and ATCC 43890) and *L. monocytogenes* (ATCC 7644, ATCC19113, and ATCC 19114). Bacteria were resuscitated aerobically on tryptic soy agar (TSA) for 24 h at 37°C then transferred to 50 ml of tryptic soy broth (TSB). Inoculated broth was incubated at 37°C overnight from resuscitated cultures (~10^9 CFU/ml). Cells were recovered from 10 ml broth by centrifugation (4000 ×*g*, 30 min); supernatant was discarded, and the precipitate (wet pellet) was resuspended in 0.2% peptone water (Difco, Sparks, MD, USA). This procedure was repeated 2 times to remove media components.

Media

The control (unstressed) and stressed *E. coli* O157:H7 and *L. monocytogenes* samples were 10-fold serially diluted in 0.2% peptone water and spread plated (0.1 ml) onto TSA and incubated for 2 h at 37°C to allow for adequate time for injured cells to recover. Then, a thin

layer (8 ml) of selective media was overlaid onto TSA and the plates were incubated for additional 22-46 h at 37°C [29]. This step was taken to preclude the growth of other bacteria. Selective m-Endo agar LES (Difco) was used for *E. coli* O157:H7 and PALCAM agar (Difco) for *L. monocytogenes*.

Antimicrobial treatments with garlic concentrate and diallyl constituents

Fresh garlic products was purchased from Global Farms Enterprises, Inc. (Los Angeles, CA, USA), stored at ca. 22°C and used within 2 weeks. Garlic juice was produced aseptically from peeled cloves using a juice extractor (WARING PRO®). The fresh garlic juice (50 ml) was immediately centrifuged at 4000 ×*g* for 10 min at 22°C. The supernatant was filtered under vacuum through: polycarbonate 10.0 micron pore size membrane (K99CP04700, GE Water & Process Technologies, Trevose, PA, USA) then a 1 micron (K10CP04700s) and finally a 0.4 micron membrane (K04CP04700) to remove potential microbial contamination to prepare the garlic concentrate. This whole process was completed within 30 minutes. The concentrate was stored at 4°C and protected from UV light. The concentrate was added into sterile tryptic soy broth (TSB) within 30 minutes to avoid the loss of volatile organosulfur compounds.

Garlic concentrate was diluted to 0, 25, 50, 75, 100 and 200 l/ml in 100 ml TSB. Diallyl sulfides (5, 10 and 20 μM) were also added into 100 ml TSB. Garlic and/or diallyl sulfide TSB was inoculated (1 ml ca. 10^7 CFU/ml of either *E. coli* O157:H7 or *L. monocytogenes* cocktail to achieve an initial inoculation level of ca. 10^5 CFU/ml. Each sample was mixed well by vortexing, then incubated at 4, 22 and 35°C for 0, 1, 3, 5 and 7 days for garlic treated and 0, 1, 2, 3, 4, 5, 6 and 7 days for diallyl sulfide treated cell suspensions. At each sampling time, the samples were serially diluted with 2% (w/v) sterile buffer peptone water and the appropriate dilution was spiral plated onto TSA and then the overlay method as described above. After incubation at 37°C for 24-48 h, viable cells were determined. All treatments were performed in triplicate (N=3).

Measurement of total phenolic content and total antioxidant capacity

Two grams of chopped garlic was extracted with 15 ml methanol under magnetic stirring for 2 h at room temperature (ca. 22°C). The extract was centrifuged at 4000 ×*g* for 20 min and the supernatant filtered. The extraction procedure was repeated three times and supernatants pooled together. The dry weight of the extracts was determined and test samples standardized to 1 mg dry matter/ml (N=2). Total phenolic content (Folin-Ciocalteu method) and antioxidant capacity (DPPH method) [30] were determined.

Electron Microscopy

Scanning electron microscopy (SEM) and trans mission electron microscopy (TEM) were performed to examine morphological changes of *E. coli* O157:H7 and *L. monocytogenes* cells before and after treatment with garlic-derived organosulfur compounds (10 μM diallyl sulfide) [SEM: FEI Quanta 200F Field Emission scanning electron microscope (Field Emission Instruments, Hillsboro, OR, USA) using an accelerating voltage of 30 kV; TEM: Philips electron microscope (Field Emission Instruments, Hillsboro, OR, USA) operated at 200 kV].

FT-IR spectroscopy analysis

At the end of each treatment, 100 ml of each bacterial culture was recovered by centrifugation at 5000 rpm for 10 min. The supernatant was discarded and the pellet resuspended in 100 ml 0.85% sterile saline. This procedure was repeated again to remove media components. Then, 100 ml was filtered through an aluminum oxide membrane filter

(0.2 μm pore size, 25 mm OD) (Anodisc, Whatman Inc., Clifton, NJ, USA) using a Whatman vacuum glass membrane filter holder (Whatman catalog no. 1960-032) to harvest bacterial cells. The anodisc membrane filter does not contribute spectral features between the wavenumbers of 4000 to 1000 cm^{-1} and provides a smooth and flat surface onto which the bacterial film can form [31]. The anodisc filters were then removed from the filtration apparatus and air dried under laminar flow at room temperature (ca. 22°C) for 60 min.

FT-IR spectra were collected using a Nicolet 380 FT-IR spectrometer (Thermo Electron Inc., San Jose, USA). The aluminum oxide membrane filter coated with a uniform and thin layer of bacterial cells was placed in direct contact with the diamond crystal cell (30,000–200 cm^{-1}) of the attenuated total reflectance (ATR) cell. Infrared spectra were recorded from 4002 to 399 cm^{-1} at a resolution of 4 cm^{-1}. Each spectrum was acquired by adding together 32 interferograms. Six spectra were acquired at room temperature (22°C) for each sample (N=3). Spectra from the first two experiments were used to establish chemometric models and the spectra from the third experiment were used for model validation.

Raman spectroscopy

A WITec alpha300 Raman microscope (WITec, Ulm, Germany) equipped with a UHTS-300 spectrometer was used in this study. This system is equipped with a 532-nm laser source and a 785-nm laser source. During the measurement, the 532-nm laser was focused onto the sample at a microscope scanning stage through a 100× objective (Nikon, Melville, NY, USA). Raman scattering spectra were detected by a 1600 × 200 pixel CCD array detector. The size of each pixel was 16 × 16 m. Spectral data were gathered in WITec Project software v2.02 (WITec, Ulm, Germany). Spectra of each bacteria sample were collected with a simultaneous detection range from 3700 to 200 cm^{-1} in the extended mode. For measurements at a single location, each full spectral measurement was conducted with a 1-s integration time with 50 spectral accumulations and approximately 2 mW incident laser power. Spectral data were taken from sample at specific wavenumbers in the so-called fingerprint region (300 to 1800 cm^{-1}). Full area scans were also performed to create Raman maps, with single spectrum integration times of 100 ms, saving 15,000 spectra acquired over a regularly spaced array of sample locations in a grid pattern (150 by 100 arrays).

Klarite™ (Renishaw Diagnostics, Glasgow, UK) SERS-active substrates were used in this study. These substrates were fabricated on silicon wafers coated with gold. Treated microbial cells (10 μl) were deposited onto the substrate for Raman measurements taken after 2 h drying under a fume hood at ca. 22°C.

Chemometric analysis and statistical analysis

Vibrational (both infrared and Raman) spectra were firstly pre-processed by EZ OMNIC 7.1a (Thermo Electron Inc.). The raw spectra were subtracted from relative background (control, aluminum membrane filter coated with residue after filtration). Then, automatic baseline correction was employed to flatten baseline, following by a smooth of 5 (Gaussian function of 9.643 cm^{-1}). The preprocessed spectra were read by Excel (Microsoft Inc., Redmond, WA). The height and area of spectral bands were measured and calculated by OMNIC and Origin® 8.1 (OriginLab Co., Northampton, MA). Second derivative transforms using a 9-point Savitzky-Golay filter and wavelet transforms (with a scale of 7) were performed for spectral processing in Matlab to enhance the resolution of superimposed bands and to minimize problems from unavoidable baseline shifts. The reproducibility of vibrational spectra from three independent experiments was investigated by calculating D_{y1y2} [32]. The comparison of spectra was performed by calculating selectivity (S) that indicates the spectral variations between reference samples (control garlic concentrate) and actual samples (bacterial-inoculated garlic concentrate) [27].

Chemometric models were established based on processed spectra, including cluster analysis (principal component analysis, PCA), dendrogram analysis (discriminant function analysis, DFA), class analog analysis (soft independent class of analog, SIMCA) and partial least squares regression (PLSR). PCA is used to reduce the dimensionality of multivariate data while preserving most of the variances. Those selected unrelated principal components (PCs) are plotted and visualized in cluster forms [14]. DFA can construct branched dendrogram structures with prior knowledge of biological sample's information [12]. SIMCA is a supervised classification method. The test samples are compared to study the degree of analogy with those of the training set of samples [32]. A combination of different chemometric models can improve selectivity and sample differentiation. The PLSR was employed for quantitative analysis using Matlab. A total of 18 spectra from each bacterial sample were used to establish the calibration model. A leave-one-out cross validation was performed to evaluate the prediction power of the model by removing one sample from the data set at a time and applying a calibration to the remaining standards. The suitability of the developed models for predicting viable *E. coli* O157:H7 and *L. monocytogenes* concentrations was assessed by regression coefficient (R), latent variables, the root mean square error of estimation (RMSEE), and the root mean square error of cross validation (RMSECV) [27]. The overall suitability of the prediction models for bacterial concentration was evaluated from the residual prediction deviation (RPD) values. The wavenumbers between 1800 cm^{-1} and 900 cm^{-1} were selected for infrared based chemometric analyses and the wavenumber between 1800 cm^{-1} to 400 cm^{-1} were selected for Raman based chemometric analyses.

Three independent trials were conducted. The results were expressed as the mean of 3 independent replicates ± standard deviation. The significant difference ($P < 0.05$) of band areas from raw spectra and second derivative transformed spectra was determined by one-way analysis of variance (ANOVA) following T-test in Matlab.

RESULTS AND DISCUSSION

Inhibitory effects of garlic concentrate and organosulfur compounds on *E. coli* O157:H7 and *L. monocytogenes*

Organosulfur compounds and polyphenols have both antimicrobial and antioxidant activity and these two properties are related to each other [7]. The total phenolic content (TPC) of garlic extract is 3.11 ± 0.33 mg GAE/g DW and total antioxidant capacity (TAC) measured as the DPPH radical is 0.91 ± 0.23 mg Trolox/g DW. The purity and stability of diallyl sulfide was monitored throughout the study by HPLC maintained at 97%. The decrease of TPC and TAC and decomposition of diallyl sulfide occurred at 4°C without light exposure but only following a long storage period of 3–4 months. Purified organosulfur compounds were used within 2 weeks and fresh garlic extract was prepared and used daily.

The effect of garlic concentrate (Supporting Information Table S1 and Table S2) and garlic derived organosulfur compounds (Supporting Information Table S3 and Table S4) on the growth of *E. coli* O157:H7 and *L. monocytogenes* was investigated at different temperatures over 0, 1, 3, 5 and 7 days. The bactericidal effect is approximately proportional to garlic and diallyl sulfide concentration and treatment time intervals. Garlic concentrate was not an effective antimicrobial for either microbe at 4°C. *L. monocytogenes* demonstrated a higher resistance to garlic and diallyl sulfide than *E. coli* O157:H7.

A concentration of 10 M of diallyl sulfide effectively eliminated *E. coli* O157:H7 in broth at 22°C at 6 days and *L. monocytogenes* in broth at 22°C at 7 days. This concentration of diallyl sulfide was effective against *E. coli* O157:H7 but not *L. monocytogenes* at 4°C. The diallyl sulfide content (10 M) used in this study was equivalent to 250-480 g/kg garlic or 18-34 fresh cloves (10 ml). Previous sensory studies using 10 M diallyl disulfide did not

produce a marked off aroma in ground beef while a strong garlic smell remained at an equivalent concentration of garlic extract [7]. Organosulfur compounds provided significant antioxidant capacity and the use at these concentrations in various food systems should be safe and acceptable in savory and moderate to highly flavored meat or vegetable based foods. In addition, diallyl sulfide components (diallyl sulfide, diallyl disulfide and diallyl trisulfide) compose approximately 80% of commercial garlic oil) and significant antimicrobial effects of these organosulfur compounds may partially explain the antimicrobial effect of commercial garlic oil [5].

FT-IR and Raman spectral features of *L. monocytogenes* and *E. coli* O157:H7

Complementary information on fundamental vibrational modes can be obtained from mid-IR and Raman spectra, as some vibrational motions are detected primarily with IR radiation and others primarily by Raman scattering with band assignments determined from earlier studies: Naumann (2001), Movasaghi et al. (2007), Movasaghi et al. (2008) and Lu et al. (2011c) [18, 32-34] and summarized in Supporting Information Table S5. Infrared and Raman spectral features of *L. monocytogenes* and *E. coli* O157:H7 intact cells are shown in Figure 1 (a) and (b).The wavenumber region below wavenumber of 1800 cm^{-1}, in both FT-IR and Raman spectra provided detailed information about composition of bacterial cells.

Raman fingerprint provided a greater number of features for the bacterial cell membrane than FT-IR, but FT-IR bands were more intense at lower wavenumbers (1000–1100 cm^{-1}) and less intense at higher wavenumbers (1200–1400 cm^{-1}). Raman scattering relies on changes in the polarizability of functional groups as atoms vibrate while IR absorption requires a change in the intrinsic dipole moment to occur with molecular vibrations [18]. Polar groups such as C=O, N-H and O-H have strong IR stretching vibrations and nonpolar groups such as C-C and S-S have intense Raman bands [20, 31].

Raman mapping and spectral reproducibility studies

Raman mapping combines the visual perception of microscopic digital imaging with Raman spectroscopy, creating a 3D spatially-accurate Raman scattering map or micrograph localized to the diffraction limit at a specific wavenumber [13, 14]. Infrared spectroscopy can only determine bulk bacteria properties due to the illumination spot size and optical configuration; whereas confocal Raman microscopy can spectral information on single bacterial cells[16]. The Raman maps of *E. coli* O157:H7 and *L. monocytogenes* are in Figure 2.

The first Raman map shows an example of a single-band spectral area plotted as a function of location; this analysis demonstrates how the sample plane begins at the optimal focal distance (top of map, highest intensities) and gradually falls out of focus as scanning continues (towards the bottom of map with decreasing intensities). The other four maps—two for each bacterium—illustrate the general variability across the fingerprint region of the Raman spectra resulting from morphological variation across the field of randomly positioned bacterial cells. Collectively, these maps are useful for quantifying the relative experimental effects due to the improbability of perfectly focusing on the membrane of a single bacterium at will.

The reproducibility of both FT-IR and Raman spectra from three independent experiments were calculated using the Pearson coefficient (expressed as D_{y1y2} value). Mean D values between 7 and 10 are considered normal when analyzing the first or second derivative of samples prepared from cultures grown in independent assays and others asserted that D values can be as high as 300 when microorganisms from different genera are compared [32]. The D value of FT-IR spectra of microorganisms is related to following factors:

wavenumber region (window) and culture age. Firstly, five windows were selected to calculate and compare D value: (1) whole wavenumber region (3300 to 900 cm^{-1}, w_1), (2) 3000-2800 cm^{-1} (fatty acids, w_2), (3) 1800-1500 cm^{-1} (proteins and peptides, w_3), (4) 1500-1200 cm^{-1} (mixed region of proteins, fatty acids and other phosphate-carrying compounds, w_4) and (5) 1200-900 cm^{-1} (carbohydrate, w_5). For *E. coli* O157:H7, the low D values were obtained from w_1 (17.35±1.28 to 24.59±1.93), w_4 (12.39±1.03 to 18.43±2.18) and w_5 (18.49±1.22 to 22.41±2.26) and high D values were obtained from w_2 (72.23±10.32 to 86.56±15.14) and w_3 (63.92±12.33 to 79.17±13.49). For *L. monocytogenes*, the low D values were obtained from w_1 (11.21±0.98 to 14.12±1.32), w_2 (18.29±1.57 to 20.95±2.01), and w_5 (15.56±1.38 to 19.42±2.09) and high D values were obtained from w_3 (57.92±11.16 to 68.39±14.93) and w_4 (67.95±16.37 to 81.32±19.89). These results were acceptable and a bit higher since a cocktail rather than a single strain was used. The incubation time and its effect on spectral variation was also investigated and spectral reproducibility was consistent when the bacteria were cultivated within 20 h and longer cultivation time increased the D value tremendously (higher than 300). For both *E. coli* O157:H7 and *L. monocytogenes*, the shape of the cell and chemical composition change as the culture become old and both factors can significantly affect the reproducibility of vibrational spectral features [32].

The D value of Raman spectra of *E. coli* O157:H7 and *L. monocytogenes* was calculated only using 1800-400 cm^{-1} because of the large number of spectral features for analysis. The D values are 5.47±0.12 to 9.18±0.69 for *E. coli* O157:H7 and 2.39±0.25 to 7.37±0.79 for *L. monocytogenes* at 20 h cultivation time indicating that the consistency of Raman spectra is higher than FT-IR spectra. The reproducibility of Raman spectra was similar to FT-IR for different cultivation times. When incubation times are greater than 20 h, spectral variation increased significantly ($P < 0.05$) with an increase of D value (higher than 340 at 72 h). The reproducibility of Raman spectra was greater than FT-IR spectra while wavenumber (window) and cultivation time significantly affects spectral features emphasizing the need for standardized procedures for bacterial cultivation and spectral measurement.

Detection of bacterial injury

The variation of spectral features between the control (no treatment with garlic or sulfide) and garlic-untreated (sulfide-untreated) bacterial samples could be visually distinguished in second derivative transformed spectra [17, 19] and selectivity values (95% confidence interval) determined. Selectivity values greater than 1 are significant for bacterial detection [27]. The presence of overlapping clusters indicates no segregation between treatments. At a concentration of 10^5 CFU/ml, the selectivity value is higher than 1, which is in agreement with previous studies [25] indicating that 10^5 CFU is the detection limit for filtration FT-IR methods for differentiation of bacterial spectral features. Furthermore, it is worth noting that the filtration FT-IR method provided a better selectivity compared to recent magnetic bead FT-IR method for pathogenic separation from complicated food matrices, such as fresh produce and meat [26].

Diallyl sulfide (Figure 3 (a)) and garlic extract treatment (Figure 3 (b)) of ***E. coli* O157:H7** show **FT-IR** spectral variations at several of the same locations and similar treatment times, for example, to protein amide and methyl features (Table 2). Other significant spectral features associated with bacterial cell injury included changes in nucleic acid and phospholipid features (Table 2).

Some differences were observed between garlic and diallyl sulfide treatments in spectral regions associated with the C-O stretching mode of C-OH groups of serine, threonine, and tyrosine of proteins (**1164** cm^{-1}) and amide III (**1309** cm^{-1}). Proteins and phospholipids in bacterial cell membranes are the main targets attacked by plant antioxidants and these alterations to spectral features are consistent with previous findings. Band areas calculated

using OMNIC and Origin® 8.1 varied significantly ($P < 0.05$) with different treatment times. For *E. coli* O157:H7, spectral variations resulting from damage by organosulfur compounds contributed more than 80% to the total spectral variation for the garlic extract treatments.

Diallyl sulfide (Figure 3 (c)) and garlic concentrate treatment (Figure 3 (d)) of ***L. monocytogenes*** show time and concentration affects indicative of cell injury (Table 2). The differences of FT-IR spectral variation between garlic-treated and diallyl sulfide-treated were observed at amide III (**1309** cm^{-1}) with similarities in the type of cell injury observed between *E. coli* and *L. monocytogenes*. Phenolic and organosulfur compounds contribute to protein damage as observed at **1401** cm^{-1} (symmetric CH_3 bending modes of the methyl groups of proteins). Band area assessments using OMNIC and Origin® 8.1 indicated significant ($P < 0.05$) differences in the spectral features of *L. monocytogenes* indicated that organosulfur containing compounds contributed more than 75% of total affect seen for the garlic concentrate treatments.

L. monocytogenes was more resistant to cell injury from exposure to organosulfur compounds than *E. coli* O157:H7 and plating results validated this. Infrared spectroscopy results indicated that structural proteins, lipids and polysaccharides were affected. Structural proteins on the cell membrane appear to be a primary target of injury. Organosulfur compounds contributed more to antimicrobial effect against both bacteria with the remaining injury attributed to phenolic compounds.

Raman spectroscopy provided additional insight as to the causes of cell injury at the level of a single bacterial cell. In the **Raman** spectra, the diallyl sulfide (10 μM) treatment at 22°C for ***E. coli* O157:H7** (Figure 4 (a)) and Table 2 indicated that bands assigned to sulfur containing functional groups in proteins and other protein and polar lipid features were significantly altered.

For *L. monocytogenes* (Figure 4 (b)) many signs of cell damage were apparent in the sulfur region (500–700 cm^{-1}) (Table 2) affecting protein structure. Polysaccharides structures were also impacted. The significant variations in sulfur region of Raman spectra were similar for both *L. monocytogenes* and *E. coli* O157:H7. Previous studies suggest that inhibition of certain microbes is via rapid reaction of thiosulfinates with thiol groups in thiol-containing enzymes. For example, allicin and other sulfur components can freely penetrate through phospholipid bilayers and interact with the thiol-containing enzymes, causing microbial injury and death [9]. In addition, the disulfide bond in ajoene appears to be necessary for antimicrobial activity, since reduction by cysteine, which reacts with disulfide bonds, destroys its antimicrobial activity [10]. Allicin inhibits the activity of many –SH enzymes including xanthine oxidase, succinic dehydrogenase, and triose phosphate dehydrogenase [8, 9]. The –S (O)–S– group shows inhibitory effect on –SH enzymes, while –S–S–, –S–, and –SO– groups were not effective [9].

Here vibrational spectroscopy can verify bacterial inactivation from treatment with garlic extract and organosulfur compounds supporting earlier studies that protein and membrane damage are the primary factors in the inactivation of both Gram-positive and Gram-negative bacteria. *L. monocytogenes* is more resistant to garlic extract treatment than *E. coli* O157:H7. Coupling infrared and Raman spectroscopies provides a powerful method for monitoring bacterial stress and injury because some important markers (parameters), such as variation of sulfur compounds are measurable by Raman and other features such as phospholipid and secondary protein structure can be detected by FT-IR.

Electron microscopic examination of cell injury

To correlate vibrational spectroscopic data with structure changes caused by garlic derived organosulfur compounds, SEM data (Supporting Information, Figure S1) and TEM data (Figure 5) were collected for untreated and treated bacteria (10 μM diallyl sulfide) following 5 days at 22°C. Figure 5 showed that untreated cells of *E. coli* O157:H7 and *L. monocytogenes* had uniform cellular structures with well-defined membranes and little debris in the cell's surrounding environment. Exposure to organosulfur compounds resulted in morphological damage such as loss of the structural integrity of the wall, membrane, and intracellular matrix. Cell deformation, breakage of cell wall and membrane, condensation of cellular material, and presence of significant amounts of cytoplasmic material and membrane were observed from the damaged cells of *E. coli* O157:H7 and *L. monocytogenes* (Figure S1 and Figure 5).

Spectral differentiation of cellular injury

The injury levels of *L. monocytogenes* and *E. coli* O157:H7 were investigated using three different segregation models, including cluster analysis (principal component analysis, PCA), dendrogram analysis (discriminant function analysis, DFA) and class analog analysis (soft independent modeling of class analog, SIMCA). All three analyses are based upon principal component selection with PCA being a nonsupervised chemometric model and DFA and SIMCA being supervised models [15, 22]. Due to the features of high dimensional vectors for infrared and Raman spectra (wavenumber *vs.* signal intensity), major PCs extraction is important to chemometric model analysis [16, 35]. Figure S2 (Supporting Information) and Figure S3 (Supporting Information) show clear segregation of *L. monocytogenes* and *E. coli* O157:H7 samples treated with garlic-derived organosulfur compound and/or garlic concentrate during various time intervals (0, 1, 3, 5 and 7 days) at 22°C. Tight clusters (PCA) (Figure S2) and clear segregation (DFA) (Figure S3) indicated significant ($P < 0.05$) treatment differences using interclass distance ranging from 7.38 to 41.12 based upon Mahalanobis distance measurements computed between the centroids of the classes. Clusters with interclass distance values higher than 3 are believed to be significantly different from each other [32]. Class analog results provided a ~90% correction rate for data classifying was achieved for both infrared and Raman spectra. Thus, segregation models could differentiate and predict bacterial injury levels based on bacterial vibrational spectral features.

PLSR model analyses

PLSR using wavenumbers below 1800 cm^{-1} as x and an indicator variable (loading plot) as y was performed for both infrared and Raman spectroscopies for *E. coli* O157:H7 and *L. monocytogenes* to predict the level of injury between different bacterial treatments. The linear regression is shown in Figure 6 and model parameters are summarized in Table 1. Due to the limited sample numbers, leave-one-out method was performed as cross validation step. A good PLS model should have high values for R (>0.95) and RPD (>5), and low values for RMSEE and RMSECV (<1) for calibration and cross validation [27]. Furthermore, a reasonable number of latent variable (generally, <10) is desired for PLSR model to avoid overfitting[16]. FT-IR and Raman PLSR models showed promising results for predicting survival *E. coli* O157:H7 and *L. monocytogenes* exposed to garlic extracts. Both infrared and Raman based PLSR models provided similar model behavior and prediction ability on the basis of R, RPD and RMSEE (Figure 6).

CONCLUSIONS

Garlic extract and the organosulfur compounds that they contain inhibit the growth of both *E. coli* O157:H7 and *L. monocytogenes*. FT-IR and Raman spectroscopies could predict the

type and degree of cell injury providing insight into the antimicrobial mechanism of garlic extract and diallyl sulfides. Chemometric techniques could differentiate injury levels and PLSR models could be used to quantify actual bacterial survival. FT-IR and Raman spectroscopies provide complementary assessments of the antimicrobial effects and alteration to cell membrane structure providing a useful new tool to study antimicrobial effects of bioactive compounds from fruits and vegetables against important foodborne pathogens.

Supplementary Material

Refer to Web version on PubMed Central for supplementary material.

Acknowledgments

We deeply appreciated Dr. Valerie Jean Lynch-Holm who aided us with electron microscope work (sample preparation and imaging) in the Franceschi Microscopy and Imaging Center at Washington State University, Pullman. This work was supported from funds awarded to B.A.R through a USDA special food security grant and from the School of Food Science at WSU. The authors also gratefully acknowledge the support of the National Science Foundation (award DMR-0619310), USDA-NIFA grant #2010-34479-20715, and the University of Idaho Biological Applications of Nanotechnology (BANTech) Center. Research in the laboratory of M.E.K. is supported by the National Institute of Health, Department of Health and Human Services, under contract number NO1-Al-30055, and, in part, from funds provided by the School of Molecular Biosciences at WSU. We also thank Dr. Douglas Call for critical reviewing the manuscript.

References

(1). Wu VCH. Food Microbiol. 2008; 25:735–744. [PubMed: 18620965]

(2). Friedman M, Henika PR, Mandrell RE. J. Food Prot. 2002; 65:1545–1560. [PubMed: 12380738]

(3). Kim JW, Kim YS, Kyung KH. J. Food Prot. 2004; 67:499–504. [PubMed: 15035364]

(4). Kyung KH, Lee YC. Food Rev. Int. 2001; 17:183–198.

(5). O'Gara EA, Hill DJ, Maslin DJ. Appl. Environ. Microbiol. 2000; 66:2269–2273. [PubMed: 10788416]

(6). Ross ZM, O'Gara EA, Hill DJ, Sleightholme HV, Maslin DJ. Appl. Environ. Microbiol. 2001; 67:475–480. [PubMed: 11133485]

(7). Yin M-C, Cheng W-S. Meat Sci. 2003; 63:23–28. [PubMed: 22061980]

(8). Feldberg RS, Chang SC, Kotik AN, Nadler M, Neuwirth Z, Sundstrom DC, Thompson NH. Antimicrob. Agents Chemother. 1998; 32:1763–1768. [PubMed: 2469386]

(9). Miron T, Rabinkov A, Mirelman D, Wilchek M, Weiner L. Biochim. Biophys. Acta. 2000; 1463:20–30. [PubMed: 10631291]

(10). Naganawa R, Iwata N, Ishikawa K, Fukuda H, Fujino T, Suzuki A. Appl. Environ. Microbiol. 1996; 62:4238–4242. [PubMed: 8900018]

(11). Call DR, Bakko MK, Krug MJ, Roberts MC. Antimicrob. Agents Chemother. 2003; 47:3290–3295. [PubMed: 14506043]

(12). Alvarez-Ordóñez A, Prieto M. Appl. Environ. Microbiol. 2010; 76:7598–7607. [PubMed: 20851964]

(13). Huang WE, Griffiths RI, Thompson IP, Bailey MJ, Whiteley AS. Anal. Chem. 2004; 76:4452–4458. [PubMed: 15283587]

(14). Jarvis RM, Goodacre R. Anal. Chem. 2004; 76:40–47. [PubMed: 14697030]

(15). López-Díez E, Goodacre R. Anal. Chem. 2004; 76:585–591. [PubMed: 14750850]

(16). Maquelin K, Choo-Smith L-P, van Vreeswijk T, Endtz HP, Smith B, Bennett R, Bruining HA, Puppels GJ. Anal. Chem. 2000; 72:12–19. [PubMed: 10655628]

(17). Schuster KC, Reese I, Urlaub E, Gapes JR, Lendl B. Anal Chem. 2000; 72:5529–5534. [PubMed: 11101227]

(18). Naumann D. Appl. Spectrosc. Rev. 2001; 36(2&3):239–298.

(19). Knauer M, Ivleva NP, Liu X, Niessner R, Haisch C. Anal. Chem. 2010; 82:2766–2772. [PubMed: 20196561]

(20). Oust A, Moretro T, Naterstad K, Sockalingum GD, Adt I, Manfait M, Kohler A. Appl. Environ. Microbiol. 2006; 72:228–232. [PubMed: 16391047]

(21). Castellano P, Vignolo G, Farias RN, Arrondo JL, Chehin R. Appl. Environ. Microbiol. 2007; 73:415–420. [PubMed: 17071790]

(22). López-Díez EC, Winder CL, Ashton L, Currie F, Goodacre R. Anal. Chem. 2005; 77:2901–2906. [PubMed: 15859609]

(23). Moritz TJ, Taylor DS, Polage CR, Krol DM, Lane SM, Chan JW. Anal. Chem. 2010b; 82:2703–2710. [PubMed: 20196565]

(24). Neugebauer U, Schmid U, Baumann K, Ziebuhr W, Kozitskaya S, Holzgrabe U, Schmitt M, Popp J. J. Phys. Chem. A. 2007; 111:2898–2906. [PubMed: 17385845]

(25). Wang H, Law N, Pearson G, van Dongen BE, Jarvis RM, Goodacre R, Lloyd JR. J. Bacteriol. 2010; 192:1143–1150. [PubMed: 20008067]

(26). Ravindranath SP, Mauer LJ, Deb-Roy C, Irudayaraj J. Anal. Chem. 2009; 81:2840–2846. [PubMed: 19281189]

(27). Davis R, Irudayaraj J, Reuhs BL, Mauer LJ. J. Food Sci. 2010; 75:M340–M346. [PubMed: 20722934]

(28). Li J, Huang Y, Ding Y, Yang Z, Li S, Zhou X, Fan F, Zhang W, Zhou Z, Wu D, Ren B, Wang Z, Tian Z. Nature. 2010; 464:392–395. [PubMed: 20237566]

(29). Kang D-H, Fung DY. J. Food Prot. 1999; 62:1346–1349. [PubMed: 10571328]

(30). Sun T, Powers JR, Tang J. Food Chem. 2007; 105:101–106.

(31). Lu X, Al-Qadiri HM, Lin M, Rasco BA. Food Bioprocess Technol. 2011c doi: 10.1007/s11947-011-0516-8, In press.

(32). Mouwen DJM, Weijtens MJBM, Capita R, Alonso-Calleja C, Prieto M. Appl. Environ. Microbiol. 2005; 71:4318–4324. [PubMed: 16085819]

(33). Movasaghi Z, Rehman S, Rehman IU. Appl. Spectrosc. Rev. 2007; 42:493–541.

(34). Movasaghi Z, Rehman S, Rehman IU. Appl. Spectrosc. Rev. 2008; 43:134–179.

(35). Moen B, Oust A, Langsrud O, Dorrell N, Marsden GL, Hinds J, Kohler A, Wren BW, Rudi K. Appl. Environ. Microbiol. 2005; 71:2086–2094. [PubMed: 15812042]

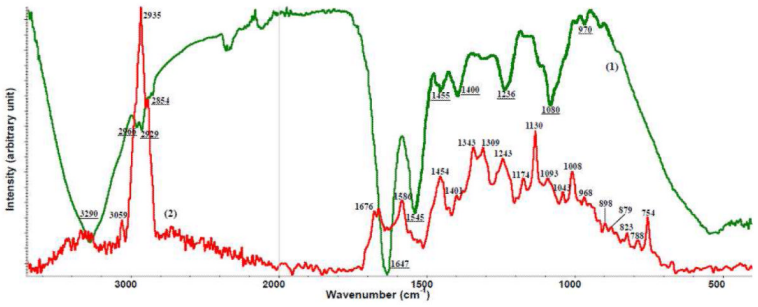

Figure 1 (a).

Different raw vibrational spectroscopic spectra of *E. coli* O157:H7 (1) IR transmission spectrum (2) micro-Raman spectrum with an excitation wavelength of 532 nm.

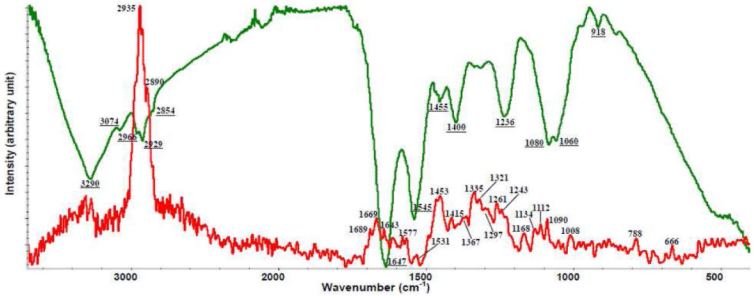

Figure 1 (b).

Different raw vibrational spectroscopic spectra of *L. monocytogenes* (1) IR transmission spectrum (2) micro-Raman spectrum with an excitation wavelength of 532 nm.

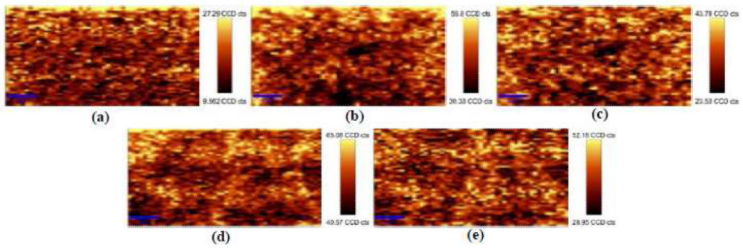

Figure 2.

Raman mapping experiment of *E. coli* O157:H7 (a-c) and *L. monocytogenes* (d-e) cells at selective wavenumbers (a) 1208-1219 cm^{-1} (b) 1195-1520 cm^{-1} (c) 1525-1788 cm^{-1} (d) 1206-1539 cm^{-1} (e) 1535-1761 cm^{-1}.

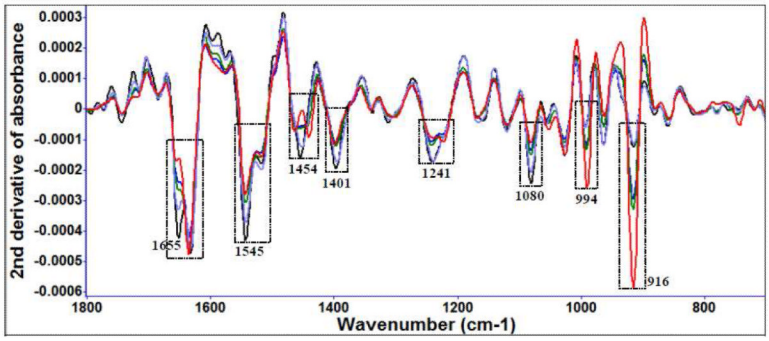

Figure 3 (a).

Second derivative transformation of FT-IR spectral features of *E. coli* O157:H7 treated with 10 μM diallyl sulfide at 22°C for different time intervals (black: 0 day, purple: 1 day, green: 3 day, blue: 5 day, red: 7 day).

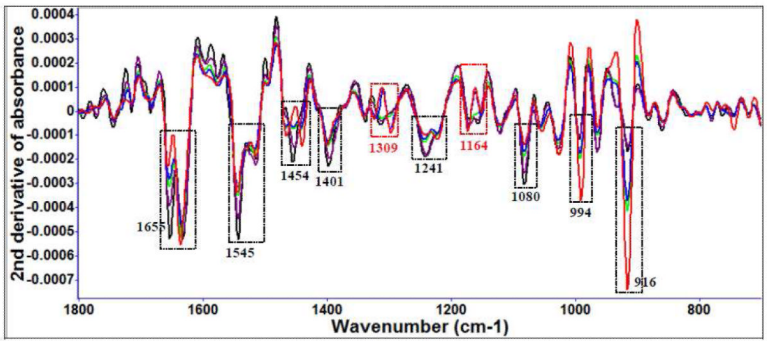

Figure 3 (b).

Second derivative transformation of FT-IR spectral features of *E. coli* O157:H7 treated with 25 μl/ml garlic concentrate at 22°C for different time intervals (black: 0 d, purple: 1 d, green: 3 d, blue: 5 d, red: 7 d). The red columns show differences in spectral features treated between garlic concentrate and organosulfur compounds.

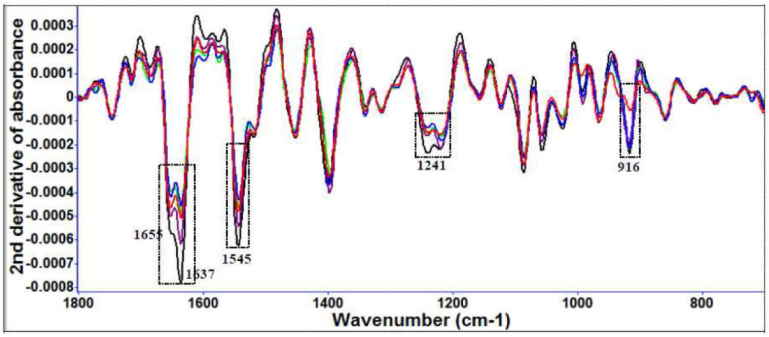

Figure 3 (c).

Second derivative transformation of FT-IR spectral features of *L. monocytogenes* treated with 10 μM diallyl sulfide at 22°C for different time intervals (black: 0 d, purple: 1 d, green: 3 d, blue: 5 d, red: 7 d).

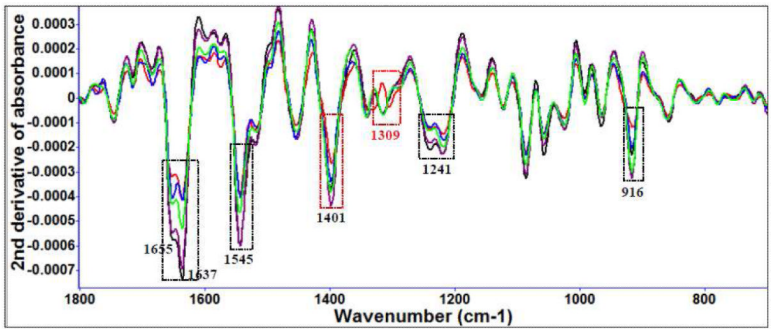

Figure 3 (d).

Second derivative transformation of FT-IR spectral features of *L. monocytogenes* treated with 25 μl/ml garlic concentrate at 22°C for different time intervals (black: 0 d, purple: 1 d, green: 3 d, blue: 5 d, red: 7 d). The red columns show differences in spectral features treated between garlic concentrate and organosulfur compounds.

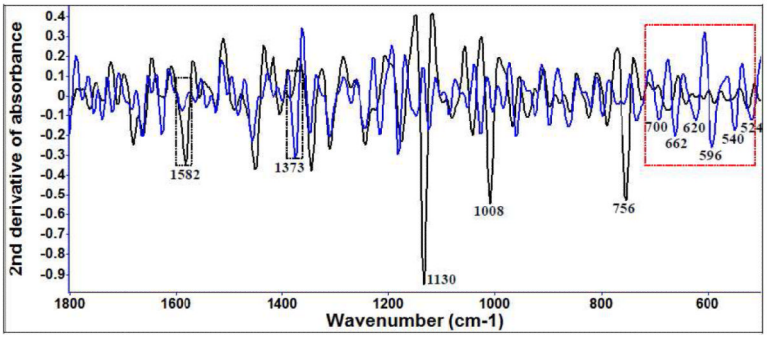

Figure 4 (a).

Second derivative transformation of Raman spectral features of *E. coli* O157:H7 treated with 10 μM diallyl sulfide at 22°C for different time intervals (blue: treated for 5 days; black: control).

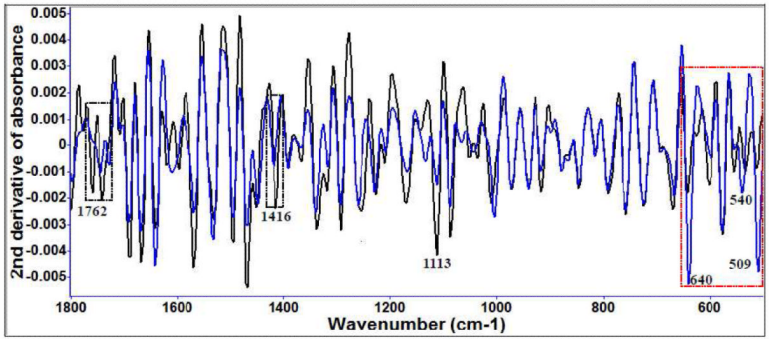

Figure 4 (b).
Second derivative transformation of Raman spectral features of *L. monocytogenes* treated with 10 μM diallyl sulfide at 22°C for different time intervals (blue: treated for 5 days; black: control).

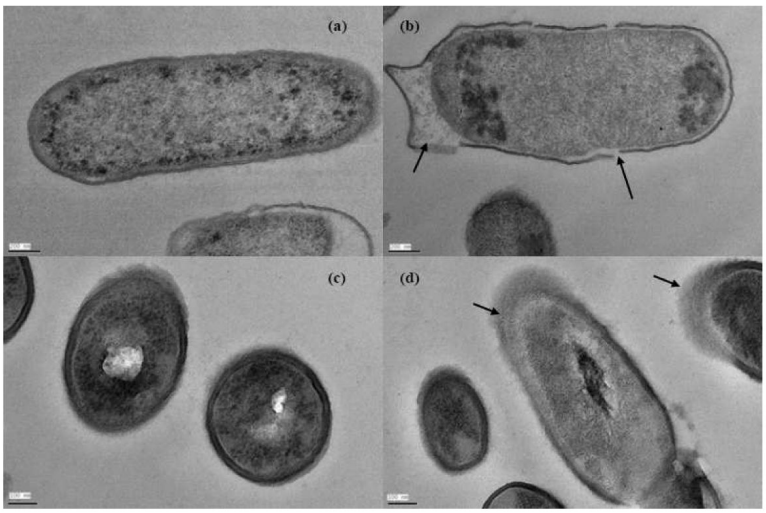

Figure 5.
Transmission electron microscope images of *Escherichia coli* O157:H7 without (a) and with (b) the treatment of organosulfur compounds derived from garlic (*Allium sativum*) and *Listeria monocytogenes* without (c) and with (d) the treatment of organosulfur compounds derived from garlic (*Allium sativum*).

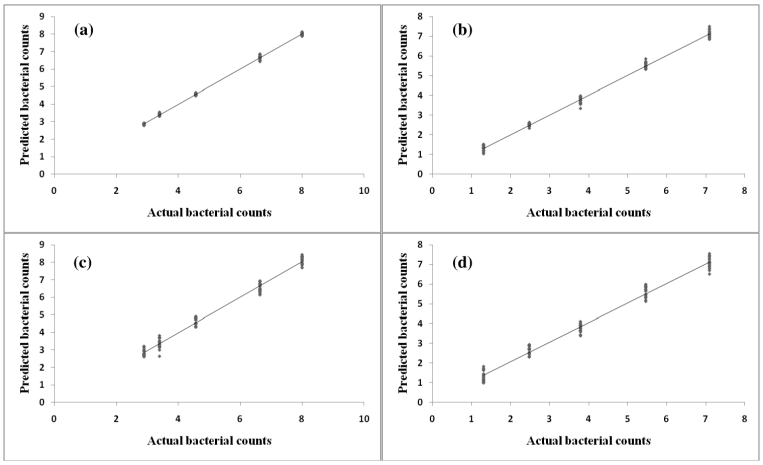

Figure 6.

Representative partial least squares regression for actual bacteiral survivial counts prediction in sterilized broth containing 10 μM diallyl sulfide for different time intervals at room temperature (22°C) for *L. monocytogenes* (a) and *E. coli* O157:H7 (b) using Raman spectra and *L. monocytogenes* (c) and *E. coli* O157:H7 (d) using infrared spectra.

Table 1

Partial least squares regression models for quantification of live pathogenic strains treated with garlic derived organosulfur compounds (10 μM diallyl sulfide) in sterilized broth.

Spectra	Range	No. of Samples	Latent Variables	R-Cal#	RMSEE-Cal	RPD-Cal	R-Val*	RMSEE-Val	RPD-Val
Listeria FT-IR	2.85-8.03	90	8	≥ 0.96	≤ 0.16	≥ 17.55	≥ 0.92	≤ 0.31	≥ 10.73
Listeria Raman	2.87-7.96	90	7	≥ 0.99	≤ 0.23	≥ 12.11	≥ 0.96	≤ 0.42	≥ 8.97
E. coli FT-IR	1.28-6.89	90	7	≥ 0.95	≤ 0.32	≥ 20.91	≥ 0.91	≤ 0.52	≥ 15.28
E. coli Raman	1.32-7.01	90	7	≥ 0.99	≤ 0.27	≥ 14.46	≥ 0.97	≤ 0.40	≥ 10.83

Note: #Cal: calibration;

*Val: validation. For FT-IR, the wavenumber 1800 to 700 cm^{-1} was used for model analyses; for Raman, the wavenumber between 1800 to 400 cm^{-1} was used for model analyses.

Table 2

Band assignments for bacterial injury from diallyl sulfide and garlic extract

Bacteria	Antimicrobials	Cellular Structures Affected	FTIR Band Assignment		Raman Band Assignment	
E. coli O157:H7	Diallyl sulfide	Proteins	amide I of α-helical structure	**1655** cm^{-1}	S-S disulfide stretch in proteins	**524** cm^{-1}
			amide II	**1545** cm^{-1}	*ν*(S-S) trans-gauche-trans (amino acid cysteine)	**540** cm^{-1}
			sym bending modes of methyl groups in skeletal proteins	**1455** cm^{-1}	C-C twist aromatic ring	**620** cm^{-1}
			asym CH_3 bending of the methyl groups of proteins	**1449** cm^{-1}	C-S stretch mode of cysteine	**662** cm^{-1}
			sym CH_3 bending modes of the methyl groups of proteins	**1401** cm^{-1}	*ν*(C-S) trans (amino acid cysteine)	**700** cm^{-1}
					sym breathing of tryptophan	**756** cm^{-1}
					phenylalanine	**1008** cm^{-1}
					tyrosine	**1373** cm^{-1}
					phenylalanine	**1582** cm^{-1}
		Lipids	CH_2 scissoring mode of the acyl chain of lipids	**1465** cm^{-1}	phosphatidylinositol	**596** cm^{-1}
			sym stretch of phosphate groups in phospholipids	**1224** cm^{-1}	phospholipid	**1130** cm^{-1}
			sym phosphate stretching mode of phosphodiesters	**1080** cm^{-1}		
			phosphodiester	**916** cm^{-1}		
		Nucleic	acids asym phosphate stretch from phosphodiester groups of cellular nucleic acids	**1241** cm^{-1}	ND	
			C-O ribose and C-C	**994** cm^{-1}		
	Phenolics	Proteins	C-O stretch mode of C-OH groups of serine, threonine, and tyrosine	**1164** cm^{-1}	ND	
			amide III	**1309** cm^{-1}		
	Diallyl sulfide	Proteins	amide I of *α*-helical structure	**1655** cm^{-1}	S-S disulfide stretch	**509** cm^{-1}
			amide I of *β*-sheet structures	**1637** cm^{-1}	*ν*(S-S) trans-gauche-trans (amino acid cysteine)	**540** cm^{-1}
			amide II	**1545** cm^{-1}	C-S stretch of proteins	**640** cm^{-1}
		Lipids	phosphodiester	**916** cm^{-1}	ND	

Bacteria	Antimicrobials	Cellular Structures Affected	FTIR Band Assignment		Raman Band Assignment	
L. monocytogenes	Phenolics	Nucleic acids	asym phosphate stretch from phosphodiester groups of cellular nucleic acids	**1241** cm^{-1}	ND	
		Proteins	amide III	**1309** cm^{-1}		
			sym CH_3 bending modes of methyl groups of proteins	**1401** cm^{-1}	ND	
		Lipids	ND		C=O stretch	**1762** cm^{-1}
		Polysaccharides	ND		saccharide	**1113** cm^{-1}
					ring structures	**1416** cm^{-1}

* note: sym: symmetric; asym: antisymmetric; ND: non detected